Magnetic correlations in $YBaCo_4O_7$ on kagome and triangular lattices

Minoru Soda,[1,2,3] Shinichi Itoh,[4] Tetsuya Yokoo,[4] Georg Ehlers,[5] Hazuki Kawano-Furukawa,[1,2] and Takatsugu Masuda[3]

[1]*RIKEN Center for Emergent Matter Science (CEMS), Wako, Saitama 351-0198, Japan*

[2]*Department of Physics, Advanced Sciences, G.S.H.S. Ochanomizu University, Tokyo 112-8610, Japan*

[3]*Neutron Science Laboratory, Institute for Solid State Physics, The University of Tokyo, Tokai, Ibaraki 319-1106, Japan*

[4]*Institute of Materials Structure Science, High Energy Accelerator Research Organization (KEK), Tsukuba, Ibaraki 305-0801, Japan*

[5]*SNS Project, Oak Ridge National Laboratory, Oak Ridge, Tennessee 37831-6475, USA*

(Received 12 March 2020; revised manuscript received 13 May 2020; accepted 17 June 2020; published 29 June 2020)

Magnetic correlation in $YBaCo_4O_7$ with kagome and triangular lattices was studied through inelastic-neutron-scattering measurements on a single crystal sample. The broad magnetic excitation was observed below 45 meV and showed dispersions both within the c plane and along the c axis. The wave vector with the minimum energy of the magnetic excitation was totally different from the magnetic Bragg point. Our analysis with the first-moment-sum rule suggests that Co ions in $YBaCo_4O_7$ form a unique three-dimensional network with the geometrically frustration.

DOI: 10.1103/PhysRevB.101.214444

I. INTRODUCTION

Geometrically frustrated magnets have been extensively investigated [1,2]. One of the three-dimensional frustrated magnets is a pyrochlore system. A three-dimensional network of vertex-sharing tetrahedra in the pyrochlore lattice forms a frustrated magnet when the nearest neighbor interactions are antiferromagnetic ones. The strong magnetic fluctuations are expected to induce a variety of the interesting magnetic properties. $Dy_2Ti_2O_7$ and $Ho_2Ti_2O_7$ are well known as a spin ice system which has no long-range order even at low temperature (T) [3]. In the similar pyrochlore system $Yb_2Ti_2O_7$, a Higgs transition from a magnetic Coulomb liquid to a ferromagnet has been reported [4]. Antiferromagnetic pyrochlore-lattice systems, such as $ZnCr_2O_4$, often have both lattice distortion and long-range magnetic ordering [5]. Geometrically frustrated magnets are good targets for studying unique magnetic properties.

The $RBaCo_4O_7$ (R = Ca, Y, and rare-earth elements) is one of geometrically frustrated systems. The $RBaCo_4O_7$ has the alternating structure of the kagome and the large triangular lattices formed by CoO_4 tetrahedra, as shown in Fig. 1(a) [6,7]. $RBaCo_4O_7$ with R^{3+} has three Co^{2+} and one Co^{3+} ions. The charge ordering has not been detected clearly, and the mixed valence with Co^{2+} and Co^{3+} is expected. The network of Co ions in $RBaCo_4O_7$ is similar to that of the tetrahedra in the pyrochlore system where the kagome and the large triangular lattices stack along the [111] direction [2]. In $RBaCo_4O_7$ the Co ions form not the tetrahedron but the hexahedron because of the different stacking of the kagome and the large triangular lattices. The large antiferromagnetic interaction estimated from the magnetic susceptibility [6,8] is expected to realize the unique magnetic property with the geometrically frustration.

In our previous study on $YBaCo_4O_7$ two transitions were found at temperatures $T_{c1} = 70$ K and $T_{c2} = 105$ K [9,10]. Below T_{c2} the magnetic reflections were observed at the $\boldsymbol{Q}$ points $(h_0 \pm 1/2, k_0, l_0)$, $(h_0, k_0 \pm 1/2, l_0)$, $(h_0 \pm 1/2, k_0 \pm 1/2, l_0)$, and $(h_0 \pm 1/3, k_0 \pm 1/3, l_0)$ (h_0, k_0, and l_0 = integers). Here the first three $\boldsymbol{Q}$ points are defined as $\boldsymbol{Q}_{1/2}$ points, and the last $\boldsymbol{Q}$ points are defined as $\boldsymbol{Q}_{1/3}$ points. Below T_{c1} the magnetic ordering grew rapidly with decreasing T. The estimated magnitudes of the magnetic moments suggest that Co ions have the high-spin state. The similar behavior with the combination of the commensurate and the incommensurate propagation vectors was also observed in $LuBaCo_4O_7$ [10,11]. On the contrary, Khalyavin *et al.* reported that the magnetic reflections in $YBaCo_4O_7$ appear only at $\boldsymbol{Q}_{1/2}$ points [12]. In the neutron diffraction experiment studied by Manuel *et al.*, the long-range ordering along the c axis and the short-range 120° configuration in the c plane were further reported just above T_{c2} [13]. The several neutron diffraction studies on single crystals $RBaCo_4O_7$ [9,11–13] have been reported, but the magnetic model in $RBaCo_4O_7$ remains controversial.

Neutron scattering is a very useful technique on the determination of the magnetic model including the magnetic correlation. Dispersive magnetic excitations in magnets give the information about the exchange interactions [14,15]. Cluster magnets produce the dispersionless magnetic excitations corresponding to the energy level [16]. In several pyrochlore and spinel systems, magnetic modes with the discrete energies have been observed in magnetically ordered phases [5,17,18]. The kagome lattice of herbertsmithite with a quantum spin-liquid state induces a gapless magnetic excitation [19]. The geometrically frustrated magnets show a wide variety of the magnetic excitation spectrum in the inelastic neutron scattering.

In this paper a neutron scattering study has been carried out on a single crystal sample of $YBaCo_4O_7$ in order to clarify the magnetic correlation in Co ions with the triangular and kagome lattices. The result reveals that the magnitude of the exchange interaction within kagome lattice is similar to that

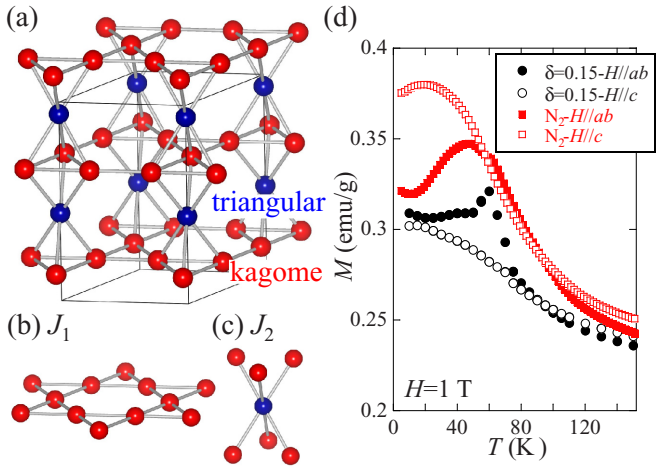

FIG. 1. (a) Schematic structure formed by Co ions in $YBaCo_4O_7$. (b) J_1 is the exchange interaction between the Co moments in the kagome lattice. (c) J_2 is the exchange interaction connecting kagome and triangular lattices. (d) Temperature dependence of the magnetization with $H = 1$ T. Closed and opened circles show the magnetization on a $\delta = 0.15$ sample with $H//ab$ plane and $H//c$ axis, respectively. Closed and opened squares show the magnetization on a N_2-annealed sample with $H//ab$ plane and $H//c$ axis, respectively.

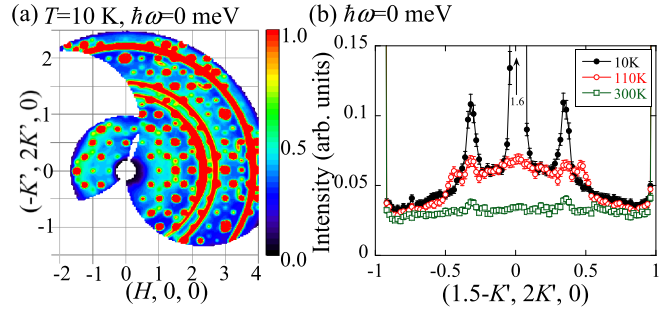

FIG. 2. Elastic neutron scattering intensities measured in a CNCS spectrometer. (a) Contour plot of the elastic neutron intensity in the $(H\ K\ 0)$ plane at $T = 10$ K. (b) Elastic neutron intensities at $(1.5 - K', 2K', 0)$ for three T values.

connecting kagome and triangular lattices. In $YBaCo_4O_7$ the exchange interactions between Co moments form the unique three-dimensional network with the geometrically frustration.

II. EXPERIMENTAL DETAILS

Single crystals of $YBaCo_4O_7$ were grown by a floating zone method. Y_2O_3, $BaCO_3$, and Co_3O_4 were mixed with proper molar ratios. The mixtures were pressed into a rod and sintered at 1000 °C for 15 h. By using the obtained rod, the $YBaCo_4O_{7+\delta}$ single crystals were grown in air, and the crystal was annealed at 1000 °C for 60 h in air. In the previous study we used the above crystal, where the oxygen content was estimated to be $\delta = 0.15$ [9]. In the present study, the crystals were reannealed at 500 °C for 60 h in nitrogen [20]. The decrease of the sample weight was 0.4(1)% by the nitrogen anneal. The single crystals were checked not to have an appreciable amount of impurity phases by a powder x-ray measurement. It should be noted that the crystal has a very slight impurity of $YBaCo_2O_{5+x}$, which shows a weak ferromagnetism between 150 and 300 K, as the previous study [9,21]. The magnetizations M were measured using a Quantum Design SQUID magnetometer under a magnetic field $H = 1$ T. The sample alignment has been carried out by using a high energy x-ray Laue system installed in ISSP, The University of Tokyo [22].

Neutron measurements were carried out by using the cold-neutron chopper spectrometer CNCS [23,24] installed at SNS, ORNL, USA, and the high resolution chopper spectrometer HRC [25] installed at MLF, J-PARC, Japan. In the measurement focusing on a low energy region at CNCS, incident neutron energy E_i was 15.1 meV, and the energy resolution at an elastic position was about $dE/E = 6\%$. The sample was cooled using a liquid helium cryostat. In the measurement focusing on a high energy region at HRC, E_i was set to 103.4 meV, and the energy resolution at an elastic position was about $dE/E = 4.5\%$. The sample was cooled using a GM-type refrigerator. For both experiments, the single crystals were oriented with the [100] and [010] axes in the horizontal plane; throughout this paper we use a hexagonal unit cell, where lattice parameters are $a = b = 6.308$ Å and $c = 10.260$ Å. The distortion of the crystal structure with orthorhombic or monoclinic symmetry has been reported [12], but we cannot discuss the correct crystal structure in the present study. Here we used the simple hexagonal unit cell without the distortion. In the expression of $\boldsymbol{Q}$ point, the $(-1, 2, 0)$ vector and its miller index K' are also used as the axis perpendicular to both a^* and c^* axes. By rotating the sample in the horizontal plane, we measured the neutron spectra in the c plane. The neutron intensities along the c axis were measured simultaneously by position-sensitive detectors settled along the vertical axis.

III. RESULTS

A. Magnetization

Figure 1(d) shows the temperature dependence of the magnetization taken at $H = 1$ T under the condition of the zero-field cooling with $H//ab$ plane and $H//c$ axis. The magnetization with the air-annealed sample ($\delta = 0.15$), which was used in the previous study [9], are also shown. By annealing the sample with N_2, the magnetization has the large change with both $H//ab$ plane and $H//c$ axis. The observed magnetization is almost consistent with that reported by Khalyavin *et al.* [12]. Furthermore, we found the 0.4(1)% decrease of the sample weight in the N_2 anneal; the ideal weight change from $\delta = 0.15$ to $\delta = 0$ is 0.42%. Then we concluded that the oxygen content of our crystal with the N_2 anneal was almost $\delta = 0$.

B. CNCS experiment in low energy region

Figure 2(a) shows the contour plot of elastic neutron intensity measured at 10 K in the $(H\ K\ 0)$ plane using the CNCS spectrometer with $E_i = 15.1$ meV. In addition to fundamental reflections and Al-powder lines, superlattice reflections were observed at both $\boldsymbol{Q}_{1/2}$ points and $\boldsymbol{Q}_{1/3}$ points although the

neutron intensities at $\boldsymbol{Q}_{1/2}$ points are much larger than those at $\boldsymbol{Q}_{1/3}$ points. This is consistent with our previous results [9]. Although the magnetic reflections at the $\boldsymbol{Q}_{1/3}$ points were not detected by Khalyavin *et al.* [12], the observation of those with even small intensities is obvious in $YBaCo_4O_7$. The profiles of the elastic neutron intensities along $(1.5-K', 2K', 0)$ at 10, 110, and 300 K are also shown in Fig. 2(b). Superlattice reflections were observed only at 10 K. On the other hand, the characteristic magnetic-diffuse scattering, which connects the $\boldsymbol{Q}_{1/2}$ points and the $\boldsymbol{Q}_{1/3}$ points, was observed at 110 K. This is the same as the line shape of magnetic-diffuse scattering reported by Manuel *et al.* [13]. It should be noted that we cannot observe the nuclear superlattice reflection clearly at 300 K, as shown in Fig. 2(b). Furthermore, the monoclinic distortion reported by Khalyavin *et al.* [12] cannot be detected at 10 K because the splitting of the peak is expected to be very small.

Figures 3(a), 3(b), and 3(c) display neutron spectra in the (H K 0) plane sliced at energies 4, 7, and 11 meV, respectively. The magnetic excitation has a sixfold symmetry in (H K 0) plane. It should be noted that the realization of the hexagonal symmetry is unnecessary here because the domain of the crystal structure with the monoclinic symmetry is expected at low temperature [12]. The magnetic spectra in the six-membered-ring shape with a focus on (0,0,0) and the similar spectra around (2,2,0), $(4,-2,0)$, and $(-2,4,0)$ were observed. This characteristic spectrum exists in all measured energy region $2 < \hbar\omega < 12$ meV. At $\boldsymbol{Q}$ points (2,2,0), $(4,-2,0)$, and $(-2,4,0)$ the neutron intensities induced by the phonon were also observed. Figures 3(e) and 3(f) display neutron spectra sliced at energy 4 meV at 110 and 300 K, respectively. Even above T_{c2} the similar magnetic spectra in the six-membered-ring shape were observed.

The inelastic neutron spectra along the (H,0,0) at 10, 110, and 300 K are shown in Figs. 3(d), 3(g), and 3(h), respectively. The magnetic excitation intensity at 10 K has a broad maximum at around $\boldsymbol{Q} = (1.25, 0, 0)$ and $\hbar\omega = 3.5$ meV, indicating that the energy gap exists at low T. This $\boldsymbol{Q}$ point with the strong intensity is different from the magnetic Bragg point (1.5,0,0). The magnetic excitation at around $\boldsymbol{Q} = (1.25, 0, 0)$ is very similar to that of $Y_{0.5}Ca_{0.5}BaCo_4O_7$ [26]. In all measurements at 10, 110, and 300 K, the neutron intensities at around $\boldsymbol{Q} = (0.8, 0, 0)$ and $\hbar\omega = 1.5$ meV remains, and the strong intensity was observed even at 300 K. Then we concluded that the intensity at around $\boldsymbol{Q} = (0.8, 0, 0)$ and $\hbar\omega = 1.5$ meV was not induced by the magnetic origin. At 110 and 300 K, the energy gap of the magnetic excitation spectrum disappears, and the large intensities from the magnetic excitation were observed even at $\hbar\omega = 0$ meV. The T dependence of the neutron spectrum at around transition temperature, where the neutron intensity is centered at $\hbar\omega = 0$, is similar to those observed in the spinel systems [5,18].

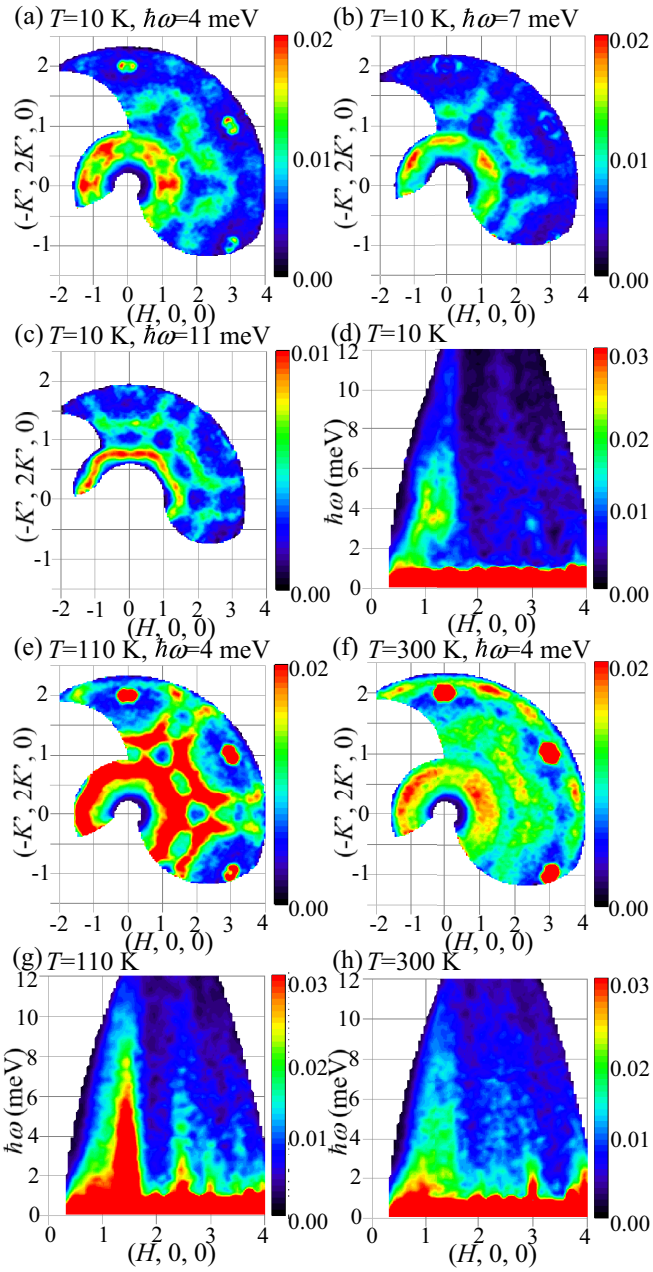

FIG. 3. Neutron scattering intensities measured in a CNCS spectrometer with $E_i = 15.1$ meV. (a)–(c) Contour plots of the inelastic neutron intensities sliced at the energies (a) 4 meV, (b) 7 meV, and (c) 11 meV in the (H K 0) plane. (d) Contour plots of the inelastic neutron intensities along the (H,0,0) at 10 K. (e) and (f) Contour plots of the inelastic neutron intensities sliced at the energies 4 meV in the (H K 0) plane at (e) 110 K and (f) 300 K. (g) and (h) Contour plots of the inelastic neutron intensities along the (H,0,0) at (g) 110 K and (h) 300 K.

C. HRC experiment in high energy region

Figures 4(a) and 4(b) show the contour plots of neutron intensities at (H,0,0) and $(-1.5, 0, L)$, respectively, measured by the HRC spectrometer with $E_i = 103.4$ meV at $T = 10$ K. The broad magnetic excitations were observed below 45 meV and the excitation energy approaches zero at around $\boldsymbol{Q} = (-1.25, 0, 0)$ although the magnetic Bragg reflection was observed at $\boldsymbol{Q} = (-1.5, 0, 0)$. This is consistent with the low energy measurement. Since the dispersions were observed both within the c plane and along the c axis, a three-dimensional network of the exchange interactions between Co moments is expected.

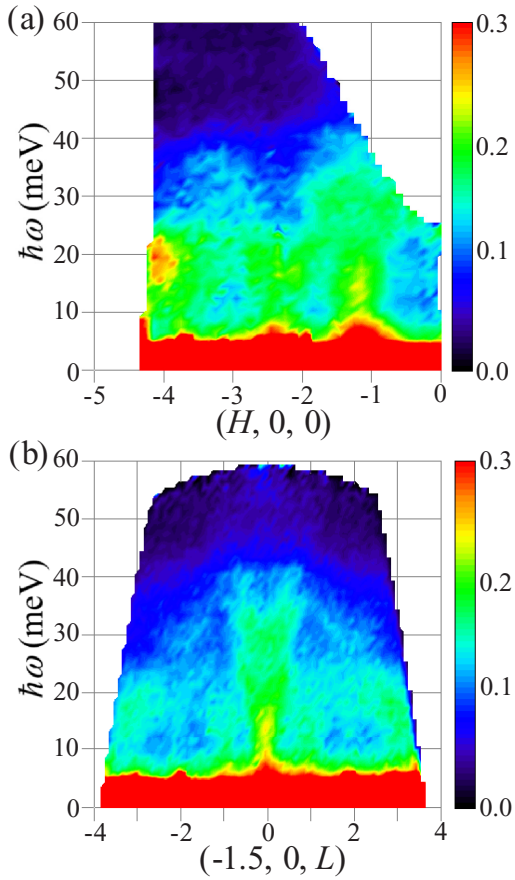

FIG. 4. Neutron scattering intensities measured in HRC spectrometer with $E_i = 103.4$ meV at 10 K. (a) and (b) Contour maps of the inelastic-neutron spectra measured at (a) (H,0,0) and (b) $(-1.5, 0, L)$.

It should be noted here the strong intensity observed at $\boldsymbol{Q} = (-4, 0, 0)$ and $\hbar\omega = 20$ meV. Figures 5(a) and 5(b) show contour plots of the neutron intensities sliced at $\hbar\omega = 20$ meV in the (H K 0) and (H 0 L) planes, respectively. At $\hbar\omega = 20$ meV the strong intensity with the same $|\boldsymbol{Q}|$ was observed for all $\boldsymbol{Q}$ directions. This means that the spotlike intensity at $\boldsymbol{Q} = (-4, 0, 0)$ and $\hbar\omega = 20$ meV is not originated from the $YBaCo_4O_7$ single crystal. Although $\hbar\omega = 20$ meV is similar to the energy of the phonon excitation in aluminum [27], which is used as the sample holder, we could not clarify the origin of the strong intensity at 20 meV. The unclear intensity observed with the same $|\boldsymbol{Q}|$ at $\hbar\omega = 20$ meV was considered as the additional background.

IV. ANALYSIS AND DISCUSSION

To discuss the magnetic model in $YBaCo_4O_7$ we employed the Heisenberg Hamiltonian,

$$\mathcal{H} = \sum_{l,m} J_{l,m} \hat{\mathbf{S}}_l \cdot \hat{\mathbf{S}}_m + \sum_{l,\beta} D_\beta \left(\hat{S}_l^\beta\right)^2. \tag{1}$$

Since the Co ions in $YBaCo_4O_7$ are located in the distorted CoO_4 tetrahedra, the electric orbital states determined by crystal field are not simple. Then, there is a possibility that the suitable model has the anisotropic exchange interaction. Above

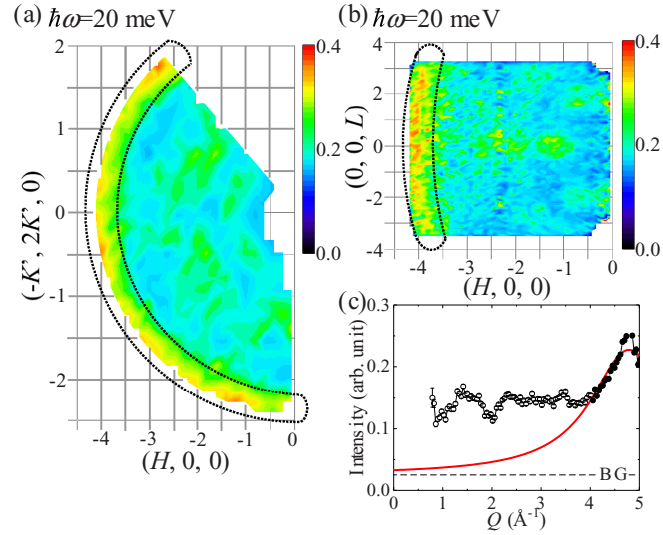

FIG. 5. (a) and (b) Contour plots of the inelastic neutron intensities sliced at $\hbar\omega = 20$ meV in (a) (H K 0) and (b) (H 0 L) planes. Strong intensities surrounded by dotted lines correspond to the additional background with $|\boldsymbol{Q}| = 4.8$ Å^{-1}. (c) Q dependence of the powder-averaged intensity at $\hbar\omega = 20$ meV. The dashed line shows the background intensity estimated in $55 < \hbar\omega < 65$ meV. The solid curve shows the additional background intensity determined by the fitting of the Lorentzian function in the high Q region. The closed circles show the data used in the Lorentzian fitting.

T_{c2}, however, the magnetizations with $H//c$ plane and $H//c$ axis show almost isotropic behavior [9,12]. Furthermore, the Heisenberg Hamiltonian without the single ion anisotropy was applied to explain the magnetic diffuse scattering of $YBaCo_4O_7$ in the Monte Carlo simulation [13]. In the present analysis, the Heisenberg spin was considered to simplify the calculation. Here the averaged magnitude of Co spin, which has the mixed valence with Co^{2+} and Co^{3+}, was considered.

We apply the first-moment-sum rule [28] because the analysis of the broad magnetic excitation, where the $\boldsymbol{Q}$ point with the minimum energy is different from the magnetic Bragg point, is difficult in the classical spin wave theory. For the spin Hamiltonian, the first-moment-sum rule can be written as

$$\int_{-\infty}^{\infty} (\hbar\omega) S^{\alpha\alpha}(\boldsymbol{q}, \omega) d(\hbar\omega) = -\frac{1}{2N} \langle [\hat{S}_{\boldsymbol{q}}^\alpha, [\hat{S}_{-\boldsymbol{q}}^\alpha, \hat{\mathcal{H}}]] \rangle = I_J^\alpha + I_D^\alpha, \tag{2}$$

$$I_J^\alpha = -\frac{1}{N} \sum_{l,m,\beta} J_{l,m} [1 - \cos(\boldsymbol{q} \cdot \boldsymbol{r}_{lm})] \times (1 - \delta_{\alpha\beta}) \langle \hat{S}_l^\beta \hat{S}_m^\beta \rangle, \tag{3}$$

$$I_D^\alpha = -\frac{1}{N} \sum_{l,\beta} D_\beta (1 - \delta_{\alpha\beta}) \times \left\{ 2 \langle (\hat{S}_l^\beta)^2 \rangle - \left[S(S+1) - \langle (\hat{S}_l^\alpha)^2 \rangle \right] \right\}, \tag{4}$$

where $S^{\alpha\alpha}(\boldsymbol{q}, \omega)$ (α and $\beta = x$, y, and z) is a dynamical structure factor. S^α is an α component of the spin operator. Since the observed magnetic excitation shows dispersions both within the c plane and along the c axis, the magnetic

excitation cannot be explained only by the magnetic interactions in the kagome lattice. Even with hexagonal space group $P6_3mc$, two kinds of bonds between Co ions within the kagome lattice and two kinds of bonds connecting kagome and triangular lattices exist. Furthermore, many kinds of bonds are expected at low temperature as the distortion of the crystal structure occurs [12]. In the present study, however, we simply consider two exchange interactions shown in Figs. 1(b) and 1(c). J_1 is the in-plane (ip) exchange interaction of $\boldsymbol{r}_1$ paths within the kagome lattice and J_2 is the out-of-plane (op) exchange interaction of $\boldsymbol{r}_2$ paths connecting kagome and triangular lattices. Although $\langle \hat{S}_l^\beta \hat{S}_m^\beta \rangle$ depends on the magnetic structure, we consider the averaged energies

$$E_{\rm ip} \equiv J_1 \overline{\langle \hat{S}_{r_0}^\beta \hat{S}_{r_0+r_1}^\beta \rangle}, \tag{5}$$

$$E_{\rm op} \equiv J_2 \overline{\langle \hat{S}_{r_0}^\beta \hat{S}_{r_0+r_2}^\beta \rangle}. \tag{6}$$

In the following analysis we focus on the $\boldsymbol{Q}$ dependence of the neutron intensity because the correct back ground is not clear. Nonetheless, Eq. (4) originating from the single-ion anisotropy has no $\boldsymbol{Q}$ dependence. This means that we cannot estimate the magnitude of the single-ion anisotropy although the energy gap was observed at low T, as shown in Fig. 3(d). Since the gap energy (∼3.5 meV) is much lower than the energy scale of the observed magnetic spectrum (∼45 meV), it is speculated that the magnitude of the single-ion anisotropy is much smaller than that of exchange interaction. In the present analysis we can determine only the ratio between $E_{\rm ip}$ and $E_{\rm op}$, which have the $\boldsymbol{Q}$ dependence.

The observed neutron intensity can be written as

$$\left(\frac{d^2\sigma}{d\Omega dE'}\right) \propto \frac{k'}{k}\{F(\boldsymbol{q})\}^2 S(\boldsymbol{q},\omega), \tag{7}$$

where k, k', and $F(\boldsymbol{q})$ are initial and final wave numbers of neutrons, and magnetic form factor, respectively [29]. By using Eqs. (2), (3), and (5)–(7), the approximate equation

$$\begin{aligned}\int_{-\infty}^{\infty} (\hbar\omega)\frac{k}{k'}\left(\frac{d^2\sigma}{d\Omega dE'}\right) d(\hbar\omega) \\ \simeq -\{F(\boldsymbol{q})\}^2 \frac{2}{N}\sum_{\boldsymbol{r}_1,\boldsymbol{r}_2}\{E_{\rm ip}[1-\cos(\boldsymbol{q}\cdot\boldsymbol{r}_1)] \\ + E_{\rm op}[1-\cos(\boldsymbol{q}\cdot\boldsymbol{r}_2)]\}\end{aligned} \tag{8}$$

can be obtained.

The contour maps of $\int_{-\infty}^{\infty}(\hbar\omega)\frac{k}{k'}(\frac{d^2\sigma}{d\Omega dE'})d(\hbar\omega)$, which is written as $\int \omega S_F$ hereafter, in (H K 0), (H 0 L), and (H H L) planes are shown in Figs. 6(a), 6(c), and 6(e), respectively. By using the neutron intensity at HRC, the energy integration was performed in the energy region $5 \leqslant \hbar\omega \leqslant 45$ meV because in the minus energy region the neutron intensity which is in proportion to the Bose factor is almost zero at 10 K, and because the influences of the Bragg intensities and the incoherent scattering exist in $-5 < \hbar\omega < 5$ meV. The $\int \omega S_F$ in (H, K,0) plane has a sixfold symmetry and the $\int \omega S_F$ along c axis also has the characteristic $\boldsymbol{Q}$ dependence.

In order to explain the $\boldsymbol{Q}$ dependences of $\int \omega S_F$ we calculated Eq. (8) with changing the ratio of $E_{\rm ip}$ to $E_{\rm op}$. For the magnetic form factor of Co ions, we used the isotropic values [30].

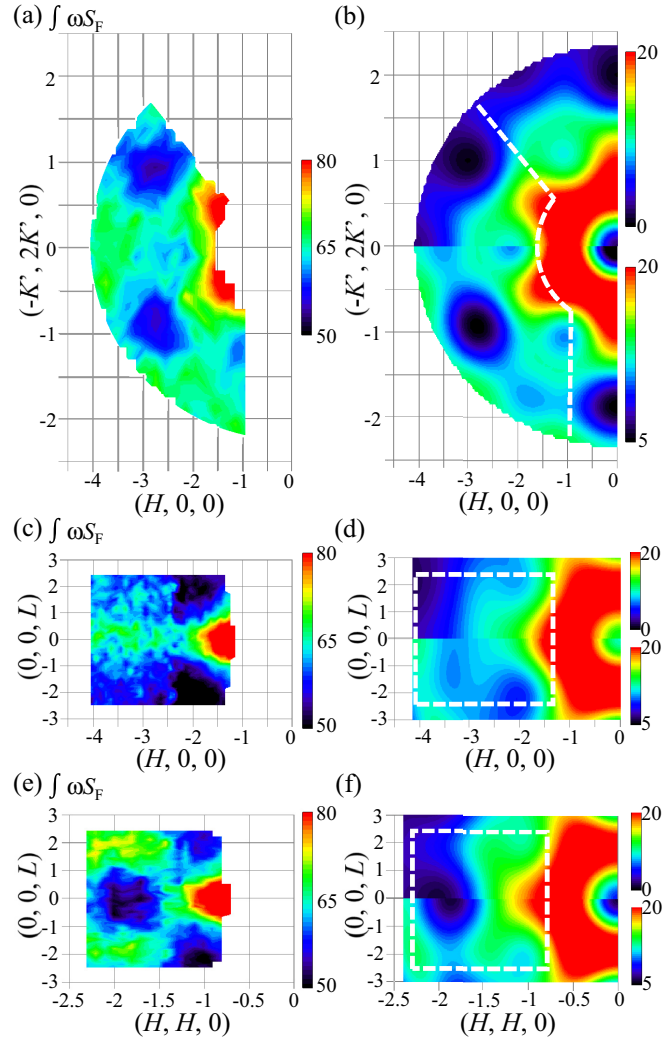

FIG. 6. (a), (c), and (e) Contour plots of $\int \omega S_F$ in (a) (H K 0), (c) (H 0 L), and (e) (H H L) planes. (b), (d), and (f) Upper half of contour plots are the calculated $\boldsymbol{Q}$ dependences of the contrast ratio with first-moment-sum rule in (b) (H K 0), (d) (H 0 L), and (f) (H H L) planes. The lower half of the contour plots are the calculated $\boldsymbol{Q}$ dependences of the contrast ratio including the additional back ground intensity. White dashed lines indicate the rough region observed in the experiment.

As the value of $E_{\rm op}/E_{\rm ip}$ was changed by 0.25 step in the range of $0 \leqslant E_{\rm op}/E_{\rm ip} \leqslant 4$, the $\boldsymbol{Q}$ dependences of $\int \omega S_F$ in all (H K 0), (H 0 L), and (H H L) planes were reproduced well for $E_{\rm ip} = E_{\rm op}$ simultaneously. The upper half in Figs. 5(b), 5(d), and 5(f) show the calculated $\boldsymbol{Q}$ dependences of the contrast ratios in Eq. (8) with applying $E_{\rm ip} = E_{\rm op}$ (<0) in (H K 0), (H 0 L), and (H H L) planes, respectively. The calculated $\boldsymbol{Q}$ dependences of the contrast ratios are roughly consistent with the observed $\int \omega S_F$.

Furthermore, we need to consider the additional background observed at around $\hbar\omega = 20$ meV. Figure 5(c) shows the $\boldsymbol{Q}$ dependence of the powder-averaged intensity at $\hbar\omega = 20$ meV. As shown by the solid line, the peak at about 4.8 Å^{-1} was fitted by Lorentzian function in the high Q region; the neutron intensity estimated in $55 < \hbar\omega < 65$ meV was used

as the background. We add the obtained Lorentzian function to the calculated $\boldsymbol{Q}$ dependences of the contrast ratios in Eq. (8). The additional background depends only on $|\boldsymbol{Q}|$ and does not affect the modulation of the intensity. The lower half in Figs. 6(b), 6(d), and 6(f) show the sum of the background intensity and the calculated $\boldsymbol{Q}$ dependences with applying $E_{\rm ip} = E_{\rm op}$ in Eq. (8) in the $(H\ K\ 0)$, $(H\ 0\ L)$, and $(H\ H\ L)$ planes, respectively. The calculated $\boldsymbol{Q}$ dependences of the contrast ratios are reproduced by the observed $\int \omega S_F$.

Neutron results suggest that the magnitude of the exchange interaction within kagome lattice is almost equal to that connecting kagome and triangular lattices. Our analysis of the inelastic neutron spectra is consistent with the estimation of the Monte Carlo simulation where the pattern of the magnetic-diffuse scattering was explained by the exchange interactions with $J_1 = J_2$ [13]. Thus, it is clear that the Co ions form the three-dimensional network of the triangles. Since the exchange interaction between Co moments is the antiferromagnetic one in $YBaCo_4O_7$ [6,8], the unique three-dimensional system with the geometrical frustration is realized. In $RBaCo_4O_7$ system, several magnetic phases, such as the multicommensurate $\boldsymbol{Q}$ [9], the single-commensurate $\boldsymbol{Q}$ [12], and the combination of the commensurate and the incommensurate $\boldsymbol{Q}$ phases [11], have been reported. The small difference of the crystal structure is expected to induce the variety of the magnetic phase because of the geometrical frustration.

From the neutron results on our $YBaCo_4O_7$ sample, where the strong intensities at both $\boldsymbol{Q}_{1/2}$ points and the weak ones at $\boldsymbol{Q}_{1/3}$ points were observed, the exchange interactions with $J_1 = J_2$ could be estimated. In the Monte Carlo simulation with $J_1 = J_2$ [13], on the other hand, the superlattice reflections at $\boldsymbol{Q}_{1/2}$ points at low temperature cannot be explained. Furthermore, the $\boldsymbol{Q}$ dependence of the magnetic excitation was different from the period of the magnetic reflections. The $(H\ K\ 0)$ contour map of the neutron intensity in the low energy region is very similar to that observed in herbertsmithite $ZnCu_3(OD)_6Cl_2$ with kagome lattice [31]. The quantum-spin-liquid state is discussed in herbertsmithite, but the similar magnetic excitation in $YBaCo_4O_7$ was observed even in the magnetic ordered phase. Furthermore, the magnetic excitation in $YBaCo_4O_7$ was explained by the network with the three-dimensional interaction. There is also a possibility that the randomness of Cu and Zn sites in herbertsmithite realizes the similar crystal structure and the similar magnetic excitation [32]. In order to clarify the origin of the broad magnetic excitation with the characteristic $\boldsymbol{Q}$ dependence in $YBaCo_4O_7$, further studies including the theoretical calculation are necessary.

V. CONCLUSION

Neutron scattering study has been carried out on a single crystal sample in order to examine the magnetic correlation in $YBaCo_4O_7$ with the kagome and the triangular lattices. The observed magnetic excitation is very broad and the $\boldsymbol{Q}$ dependence of the magnetic excitation is different from the period of the magnetic Bragg reflections. In the low energy region the $\boldsymbol{Q}$ dependence of the magnetic excitation is similar to that in herbertsmithite with the spin-liquid state. Our result suggests that the magnitude of the exchange interaction within kagome lattice is almost equal to that connecting kagome and triangular lattices. The $YBaCo_4O_7$ system is the unique three-dimensional frustrated magnet.

ACKNOWLEDGMENTS

The neutron experiment at the Materials and Life Science Experimental Facility of J-PARC was performed under the user program (Proposal No. 2014A0192). Travel expense for the neutron experiment on CNCS was supported by a General User Program for Neutron Scattering Experiments, Institute for Solid State Physics, The University of Tokyo (Proposal No. 13531 and No. 13569). The research at ORNL's Spallation Neutron Source was sponsored by the Scientific User Facilities Division, Office of Basic Energy Sciences, U.S. Department of Energy. This work was supported by KAKENHI (24740224 and 15K05123).

[1] A. P. Ramirez, Annu. Rev. Mater. Sci. **24**, 453 (1994).
[2] J. E. Greedan, J. Mater. Chem. **11**, 37 (2001).
[3] S. T. Bramwell and M. J. P. Gingras, Science **294**, 1495 (2001).
[4] L.-J. Chang, S. Onoda, Y. Su, Y.-J. Kao, K.-D. Tsuei, Y. Yasui, K. Kakurai, and M. R. Lees, Nat. Commun. **3**, 992 (2012).
[5] S.-H. Lee, C. Broholm, T. H. Kim, W. Ratcliff, and S.-W. Cheong, Phys. Rev. Lett. **84**, 3718 (2000).
[6] M. Valldor and M. Andersson, Solid State Sci. **4**, 923 (2002).
[7] M. Valldor, Solid State Sci. **6**, 251 (2004).
[8] E. V. Tsipis, D. D. Khalyavin, S. V. Shiryaev, K. S. Redkina, and P. Nunez, Mater. Chem. Phys. **92**, 33 (2005).
[9] M. Soda, Y. Yasui, T. Moyoshi, M. Sato, N. Igawa, and K. Kakurai, J. Phys. Soc. Jpn. **75**, 054707 (2006).
[10] M. Soda, Y. Yasui, T. Moyoshi, M. Sato, N. Igawa, and K. Kakurai, J. Magn. Magn. Mater. **310**, e441 (2007).
[11] M. Soda, T. Moyoshi, Y. Yasui, M. Sato, and K. Kakurai, J. Phys. Soc. Jpn. **76**, 084701 (2007).
[12] D. D. Khalyavin, P. Manuel, B. Ouladdiaf, A. Huq, P. W. Stephens, H. Zheng, J. F. Mitchell, and L. C. Chapon, Phys. Rev. B **83**, 094412 (2011).
[13] P. Manuel, L. C. Chapon, P. G. Radaelli, H. Zheng, and J. F. Mitchell, Phys. Rev. Lett. **103**, 037202 (2009).
[14] K. Matan, D. Grohol, D. G. Nocera, T. Yildirim, A. B. Harris, S. H. Lee, S. E. Nagler, and Y. S. Lee, Phys. Rev. Lett. **96**, 247201 (2006).
[15] M. Poienar, F. Damay, C. Martin, J. Robert, and S. Petit, Phys. Rev. B **81**, 104411 (2010).
[16] T. Haku, K. Kimura, Y. Matsumoto, M. Soda, M. Sera, D. Yu, R. A. Mole, T. Takeuchi, S. Nakatsuji, Y. Kono, T. Sakakibara, L.-J. Chang, and T. Masuda, Phys. Rev. B **93**, 220407(R) (2016).
[17] S.-H. Lee, C. Broholm, W. Ratcliff, G. Gasparovic, Q. Huang, T. H. Kim, and S.-W. Cheong, Nature (London) **418**, 856 (2002).

[18] K. Tomiyasu, H. Suzuki, M. Toki, S. Itoh, M. Matsuura, N. Aso, and K. Yamada, Phys. Rev. Lett. **101**, 177401 (2008).

[19] J. S. Helton, K. Matan, M. P. Shores, E. A. Nytko, B. M. Bartlett, Y. Yoshida, Y. Takano, A. Suslov, Y. Qiu, J.-H. Chung, and D. G. Nocera, and Y. S. Lee, Phys. Rev. Lett. **98**, 107204 (2007).

[20] M. Karppinen, H. Yamauchi, S. Otani, T. Fujita, T. Motohashi, Y.-H. Huang, M. Valkeapää, and H. Fjellvåg, Chem. Mater. **18**, 490 (2006).

[21] D. Akahoshi and Y. Ueda, J. Solid State Chem. **156**, 355 (2001).

[22] S. Hayashida, M. Soda, S. Itoh, T. Yokoo, K. Ohgushi, D. Kawana, and T. Masuda, Phys. Proc. **75**, 127 (2015).

[23] G. Ehlers, A. A. Podlesnyak, J. L. Niedziela, E. B. Iverson, and P. E. Sokol, Rev. Sci. Instrum. **82**, 085108 (2011).

[24] G. Ehlers, A. A. Podlesnyak, and A. I. Kolesnikov, Rev. Sci. Instrum. **87**, 093902 (2016).

[25] S. Itoh, T. Yokoo, S. Satoh, S. Yano, D. Kawana, J. Suzuki, and T. J. Sato, Nucl. Instrum. Meth. Phys. Res. A **631**, 90 (2011).

[26] J. R. Stewart, G. Ehlers, H. Mutka, P. Fouquet, C. Payen, and R. Lortz, Phys. Rev. B **83**, 024405 (2011).

[27] M. Kresch, M. Lucas, O. Delaire, J. Y. Y. Lin, and B. Fultz, Phys. Rev. B **77**, 024301 (2008).

[28] I. Zaliznyak and S. Lee, in *Magnetic Neutron Scattering in Modern Techniques for Characterizing Magnetic Materials*, edited by Y. Zhu (Springer, Heidelberg, 2005).

[29] G. L. Squires, *Introduction to the Theory of Thermal Neutron Scattering* (Cambridge University Press, Cambridge, 1978).

[30] P. J. Brown, *International Tables for Crystallography*, edited by A. J. C. Wilson (Kluwer, Dordrecht, 1992), Vol. C, Chap. 4.

[31] T.-H. Han, J. S. Helton, S. Chu, D. G. Nocera, J. A. Rodriguez-Rivera, C. Broholm, and Y. S. Lee, Nature (London) **492**, 406 (2012).

[32] H. Kawamura, K. Watanabe, and T. Shimokawa, J. Phys. Soc. Jpn. **83**, 103704 (2014).